Numerical study of liquid metal film flows in a varying spanwise magnetic field

D. Gao*, N.B. Morley, V. Dhir

Department of Mechanical and Aerospace Engineering, University of California, Los Angeles, CA 90095

Abstract

A 2D model with focus on field gradient effect is presented and explained. The numerical schemes to solve the time-dependent governing equations in volume-of-fluid (VOF) methodology are described. A model case of flow through a partially full exit-pipe between toroidal field coils, as it applies to the parameters of the APEX CLiFF-Sn concept, is explored using this tool. The results show that the field gradient restrains and destabilizes the flow, but that an applied streamwise current can propel the flow through the gradient region. A small change of the magnetic field variation with the streamwise coordinate may lead to large difference of flow behavior, and an increase in back wall electrical conductance may intensify the instability of the film flow.

*Corresponding author. Tel.: 310-206-4805; fax: 310-825-2599; email: donghong@seas.ucla.edu; mail: Mechanical and Aerospace Engineering Dept., 43-133 Engineering IV, Los Angeles, CA 90095.

1. Introduction

The proposed application[1] of liquid metal film flows on divertors and first walls to protect the plasma-facing solid structures prompts more interest on the dynamic characteristics of liquid film flows in spatially varying strong magnetic fields. Specifically, a proposed design concept being proposed by Nelson[2] in the APEX project is to use large drain duct that does dual services as a liquid drain and particle pumping port. The flow must go through a very strong toroidal magnetic field with strong field gradient in the streamwise direction. This design idea requires the liquid flow to drain by gravity or applied magnetic force while not filling up the channel, eliminating particle pumping conductance.

Our major concern analyzed here is whether film flows can overcome the field gradient to achieve a quasi-stable state with satisfactory room for particle pumping. Most previous free surface MHD flow studies consider the flow in uniform transverse magnetic field, while the effect of magnetic field gradient has received relatively less attention. Branover[3] and Leilausis[4] illustrated that the field gradient will result in induced currents in the planes parallel to the streamwise direction. This is quite different from the Hartmann type problem[3] where the induced current is in the cross sections.

Gao and Morley[5] presented a 2D model based on a 2D geometry with velocity field in x-y plane and magnetic field aligned in z-direction (spanwise). The model considers the spanwise field gradient effect and neglects the Hartmann layers effect

on the film flow, which have here been removed to infinity. A complete treatment of this problem requires inclusion of 3 components of magnetic field and the fully 3D geometry of the pipe. We have chosen to focus on just the effects resulting from the toroidal field gradient, which is a largely unexplored phenomena for open channel flows. This focus can be justified somewhat by using correlations from Morley[6] to predict the fully developed "equilibrium" film height. Purely laminar flows with no magnetic field will tend towards a flow thickness of 3 mm at the flowrates considered here. If the effect of Hartmann layers from the toroidal field is included, this film height doubles. If we consider the Hartmann layer drag from the contribution of the y-directed field this film height increases to about 18 cm. But as will be seen in the following calculations, the toroidal gradient can cause even larger film height changes, on the order of 30 cm.

In this paper, we use this model to investigate how the originally quasi-stable flow develops in a strong, spatially varying magnetic field by full-scale of direct numerical simulation of the flow in the geometry and field strength anticipated for partially-full exit-pipe flow between toroidal field coils. We include in this study an investigation of the effect of applied currents that can potentially produce a propulsion effect[7] to overcome the field gradient (diamagnetic) drag effect. In the following sections, the governing equations for the 2D MHD flows in a field gradient are presented and the numerical schemes for the free surface MHD flow are described. We will be emphasized on the presentation of results.

2. Governing equations

We consider the liquid metal layer of constant density ρ, dynamic viscosity μ, electrical conductivity σ_e, magnetic permeability μ_m, draining down a duct as shown in Fig. 1. The dynamics of the gas above the liquid is ignored, so the space occupied by the gas is taken as void. The velocity field $\vec{V} = (u, v, 0)$ is in x-y plane and the magnetic field is aligned in z-direction, also called spanwise. The spanwise magnetic field varies with x- or y-position. This applied magnetic field (B_a) gradient will interact with liquid metal movement and will produce currents in x-y plane[3, 4]. The induced currents in turn generate their own induced magnetic field B_i, which is also aligned in spanwise. We use scalar variables B_a, B_i to represent spanwise magnetic fields. The incompressible liquid metal flow is described by the time-dependent electromagnetic induction equation, momentum equations and mass conservation law[5], with focus on the magnetic field gradient effect,

$$\frac{\partial B_i}{\partial t} + (\vec{V} \cdot \nabla) B_i = \frac{1}{\mu_m} \nabla \times \left(\frac{1}{\sigma_e} \nabla \times B_i \hat{z} \right) - (\vec{V} \cdot \nabla) B_a - \frac{\partial B_a}{\partial t} \tag{1}$$

$$\frac{\partial \vec{V}}{\partial t} + (\vec{V} \cdot \nabla) \vec{V} = \frac{1}{\rho} \nabla \cdot \mathbf{T} + \vec{g} - \frac{1}{\rho \mu_m} (B_i + B_a) \nabla B_i \tag{2}$$

$$\nabla \cdot \vec{V} = 0 \tag{3}$$

where $\vec{g}$ is the gravity acceleration, $\mathbf{T} = -p\,\mathbf{I} + \mu[\nabla \vec{V} + (\nabla \vec{V})^{\mathrm{T}}]$ is the stress tensor with p the pressure and $\mathbf{I}$ the indentity tensor. The form of the induction equation, Eq. (1), reveals that the source of induced magnetic field, or in another words the electrical current, comes from the spatial or temporal variation of the applied field.

It does not depend at all on the absolute value of applied field.

Only non-ferromagnetic materials are considered. We assume a thin bottom wall with σ_w electrical conductivity and t_w thickness. The boundary condition at this thin conducting wall is

$$\frac{\sigma_w t_w}{\sigma_e}\frac{\partial B_i}{\partial y} - (B_i - B_i(y=-t_w)) = 0 \qquad \text{at } y=0 \tag{4}$$

which reduces to $B_i(y=0) = B_i(y=-t_w)$ for nonconducting wall. If no current is allowed to flow out of the bottom wall into the surrounding space then $B_i(y=-t_w)$ is constant with x. Likewise $B_i(y=h)$ is also a constant along the free surface surface contour of liquid. If an applied current I_a is allowed to flow into/out of the domain along the flow direction, then the boundary condition at the inlet/outlet will be that

$$\partial B_i/\partial y = \mu J_a, \qquad \text{at } x=0,\ x_{max} \tag{5}$$

where J_a is a given applied current density. Therefore there will be an integral contraint on the values of the constant B_i at the back wall and free surface boundaries such that

$$B_i(y=h) - B_i(y=-t_w) = \mu_m\, I_a \tag{6}$$

To facilitate the numerical implementation of the boundary condition in VOF method, the value at the bottom wall is taken as $B_i(y=-t_w) = -\mu_m\, I_a$, because the current and B_i are assigned a zero value in the void. The other boundary conditions can be summarized as: at bottom wall, non-slip condition for velocity; at inlet, fixed velocity

1.0 m/s; at outlet, continuous condition for velocity and B_i. The dynamics conditions at free surface is implemented via VOF free surface tracking numerical scheme.

3. Numerical Schemes

The numerical tool is designed for the general two-dimensional MHD flows with free surface. The numerical computation of flows with free surfaces involves two coupled tasks: (1) resolve the flow field and (2) predict the position of the free surface accurately. The first task is achieved by solving the Navier-Stokes equations via the projection method[8] technique where the pressure is decoupled from the momentum equations and is used to form the pressure Poisson equation. The pressure field is then used to correct an initial velocity prediction, thus recovering the continuity constraint. The magnetic induction equation can be solved implicitly in a fashion similar to the pressure Poisson equation, not causing additional CFL constraint.

The second task is carried out in Volume of Fluid (VOF) methodology[9]. A VOF method consists of two parts: an interface reconstruction algorithm to determine an interface from the given volume fraction data, and a VOF advection algorithm to determine the volume fraction data at the new time step from the old velocity field and the interface location. The VOF method is robust, powerful, reasonably correct, and it can avoid topological constraint. A detailed review of VOF method is available in the Rider and Kothe[10]. The dynamic condition at free surface is implemented via the continuum surface force (CSF) model[11]. In the VOF method, a scalar variable

$f(x, y, t)$ is introduced. The discrete variable $f_{i,j}$ represents the volume fraction of the cell (i, j) occupied by the fluid. For incompressible flows, mass conservation is equivalent to volume conservation, so the f is transported according to the VOF advection equation

$$\frac{\partial f}{\partial t} + (\vec{V} \cdot \nabla) f = 0 \tag{7}$$

4. Result and Discussion

The applied magnetic field varies with the streamwise distance as shown in Fig. 2. We call this the magnetic field profile in this work. Due to the numerical difficulty in calculating flows with very strong gradients, in the computational cases reported below we let $B_a = \beta *$ profile-in-Fig, where β is a scaling factor. So we essentially investigate the film flows under same field profiles but different gradient values by varying β. All the calculations use B-profile 1 except one uses B-profile 2 in order to study the field profile effect. The configuration of the flow is shown in Fig. 1, it is initialized to be quasi-stable ordinary developing flow. The liquid metal is Sn. An inlet velocity and height of 1 m/s and 0.3 m is chosen to match the outflow conditions needed in the APEX CLiFF-Sn application.

4.1. Unstable flows with increasing β factor

We first want to know how the film flow develops after a magnetic field $B_a = \beta *$ profile-1 is imposed on the initial flow with a nonconducting back wall and no

applied streamwise current. The Fig. 3 shows that at weak magnetic field gradient, here represented by β, the film flow can achieve a quasi-stable state after a short temporal development. Also the result illustrates a bulge forms for the quasi-stable MHD film flow, the bulge increases exponentially with the β. Extensive numerical experiments indicate a critical point exists at about $\beta = 0.175$; above this value the surface tension no longer overcomes the electromagnetic force, and the film flows will blow up around the field gradient region. Figure 4 displays the evolution of the flow at $\beta = 0.2$, where we see that the bulge fills the entire pipe.

The unstable flow phenomena can be understood from the interaction of liquid motion and magnetic field gradient. As an example, the induced currents at t=0.66 sec and $\beta = 0.2$ is shown in the Fig. 5. Due to the gradient of the magnetic field, the Lorentz force near the inlet side of the bulge acting to stop the flow is larger than the pushing force at far end side of the bulge due to the field gradient, and near the free surface the force is pointing upward to oppose the surface tension. The induced current is intensified by the field gradient, so the quasi-stable flows can not be obtained when increasing β over a critical value.

4.2. Influence of conducting wall and and field profile

Figure 6 provides a comparison of film flow shapes after 0.66 seconds for the conducting wall and nonconducting wall cases. Here for both cases there is no applied current and the flows starts from same initial state. The wall has same conductivity as the liquid metal and has 4 mm thickness. It can be seen the effect of the conducting

wall is to make the flow more unstable, and it is expected the magnetic effect will be enhanced as the wall/liquid conductivity parameter $\Phi = \sigma_w t_w/\sigma_e l$ increases. The conducting wall effect is understandable, because the conducting wall helps currents to find easy loop to encircle, thereby enhancing the generation of induced currents. The resulting Lorentz force is thus further augmented.

One interesting phenomena is shown in Fig. 7. Here the only difference is the field profile. The B-profile 1 and B-profile 2, as shown in Fig. 2, are quite similar; they have same maximum field gradients. The B-profile 1 decreases gradually to the zero after the field reaches its positive peak, while the B-profile 2 keeps constant after reaching the positive peak. The small difference of the B-profiles produces significantly different flow behaviors after very short developing time 0.33 sec. That is maybe due to the opposite influence of the positive field gradient and negative field gradient. Although the negative field gradient in B-profile 1 is very small, but it closely follows the big positive field gradient. The negative field gradient generates the force to push the liquid forward, that is very helpful to discharge the liquid from the bulge region. This result can give us some enlightment that a good design of divertor, although we can not avoid the field gradient, can benefit from the appropriate field profile.

4.3. Magnetic Propulsion effect of applied streamwise current

The propulsion effect of applied current is demonstrated in Fig. 8. Here the bottom wall is non-conducting. The result shows us that an appropriate applied

current can reduce the bulge, and help the flow to achieve a quasi-stable state. The propulsion effect of applied current is signified by the increased flow rate in the analysis of Gao and Morley[5]. Here the flow rate is maintained constant, but the bulge is formed due to the flow resistance from the field gradient. The applied current acts to reduce the resistance and increase the flow rate at bulge region, therefore the liquid is not restrained in this region. Figure 9 shows the development of the flow at bigger field gradient $\beta = 0.5$ after an applied current is applied. The flows first experiences a transient unstable period. When the jitters pass away with increasing I_a, a quasi-stable state can be obtained. We should be careful that lots of small disturbance or void bubbles may exist in the film flow. But as this analysis is geared towards gross flow in an exit-pipe, the surface integrity serves no role for any surface heat or radiation protection. The goal of the work is to show the field gradient effect on the gross flow, so that the fine surface features may not be accurately enough calculated. High accurate numerical surface tracking schemes are recommended for the fine feature study if it is necessary for future applications.

5. Conclusion

A 2D model with focus on the magnetic field gradient effect is presented. The numerical computation results are presented and discussed. More discussion about the results and verification of the modeling are available in Gao[12]. It is shown the magnetic field gradient effect is to oppose the flow, and make the flow unsta-

ble, causing overfilling of the exit-pipe and reduced particle pumping conductance. However, applied streamwise currents can efficiently utilize the strong magnetic field gradient to help propel the flow and overcome the field gradient drag effect. Since the condition of the surface and the velocity profile of the liquid in the exit-pipe are of little importance for any surface heat or particle protection functions, the magnetic propulsion concept of Zakharov seems ideally suited for this type of flow.

Acknowledgement

The authors would like to gratefully acknowledge the support of U.S. Department of Energy through Grand No. DE-FG03-86ER52123, and the support of fusion technology group at UCLA and Leonid Zakharov at PPPL.

References

[1] M. A. Abdou et al., On the exploration of innovative concepts for fusion chamber technology, Fusion Engineering and Design 54(2001)181-247.

[2] B. Nelson, APEX study, http://www.fusion.ucla.edu/apex.

[3] H. Branover, Magnetohydrodynamic Flows in Ducts, Israel University Press, Jerusalem, Israel, 1978.

[4] Lielausis, Liquid-Metal Magnetohydrodynamics, Atomic Energy Review, Vol.13, International Atomic Energy, Vienna, 1975, pp. 527-581

[5] D. Gao and N. B. Morley, Equilibrium and initial linear stabiblity analysis of liquid metal falling film flows in a varying spanwise magnetic field, Magnetohydrodynamics (2002) No.4, to appear.

[6] N. B. Morley and M. A. Abdou, "Study of fully developed, liquid-metal, open-channel flow in a nearly coplanar magnetic field," Fusion Tech. 31(1997)135-153.

[7] L. E. Zakharov, Magnetic propulsion of conducting fluid and the theory of controlled tokamak fusion reactor, Proc. Int. Fusion/Plasma Conference on Liquid Lithium, Controlled Tokamak Fusion Reactors & MHD, Sherwood. 1999.

[8] A. J. Chorin, Nemerical simulation of Navier-Stokes equations, Mathematics of Computation 22(1968)745-762.

[9] C. W. Hirt and B. D. Nichols, Volume of Fluid(VOF) method for the dynamics of free boundaries, Journal of Computational Physics 39(1981)202-225.

[10] W. J. Rider and D. B. Kothe, Reconstructing volume tracking, Journal of Computational Physics 141(1998)112-152.

[11] J. U. Brackbill, D. B. Kothe, and C. Zemach, A continnum method for modelling surface tension, Journal of Computational Physics 100(1992)335-354.

[12] D. Gao, Ph.D. dissertation, Mechanical Engineering Department, University of California, Los Angeles, 2002, to appear.

1 Figure captions

FIG.1

The configuration of the exit-pipe film flows.

FIG.2

The spanwise magnetic field versus x.

FIG.3

The free surfaces of the quasi-stable film flows at small β at nonconducting wall, no applied current.

FIG.4

The development of the film flow at $\beta = 0.2$, nonconducting wall, no applied current.

FIG.5

The induced current for the film flow at t=0.66 sec, $\beta = 0.2$, nonconducting wall, no applied current.

FIG.6

The comparison of film flow shapes for conducting bottom wall and nonconducting wall cases.

FIG.7

The comparison of film flow shapes when B_a is in B-profile 1 and B-profile 2. AT t=0.33 sec, $\beta = 0.2$, nonconducting wall, no applied current.

FIG.8

The propulsion effect of the applied current. At t=0.66 sec, $\beta = 0.2$, nonconducting wall.

FIG.9

The development of the film flow under propulsion effect of the applied current at large field gradient $\beta = 0.5$, $I_a = 2.5e5$A, nonconducting wall.

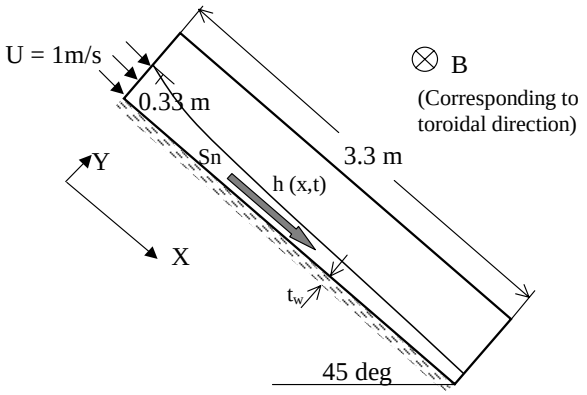

FIG. 1. The configuration of the exit-pipe film flows.

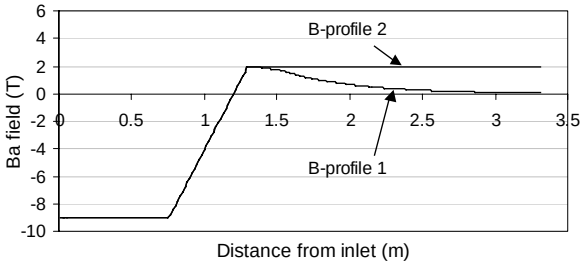

FIG. 2. The spanwise magnetic field versus x.

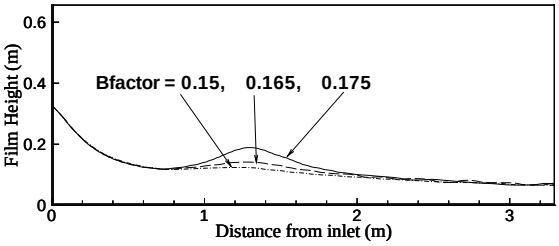

FIG. 3. The free surfaces of the quasi-stable film flows at small β at nonconducting wall, no applied current.

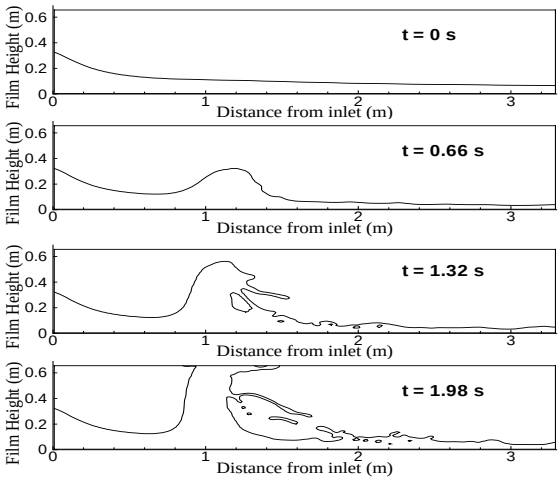

FIG. 4. The development of the film flow at $\beta = 0.2$, nonconducting wall, no applied current.

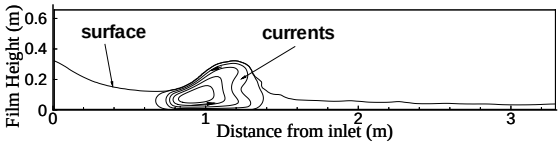

FIG. 5. The induced current for the film flow at t=0.66 sec, $\beta = 0.2$, nonconducting wall, no applied current.

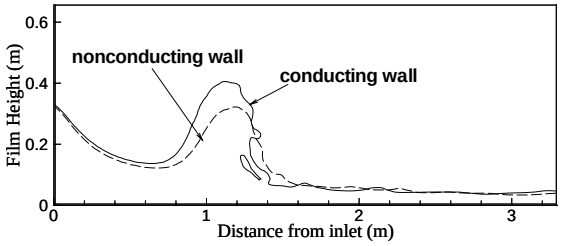

FIG. 6. The comparison of film flow shapes for conducting bottom wall and nonconducting wall cases. AT t=0.66 sec, $\beta = 0.2$, no applied current.

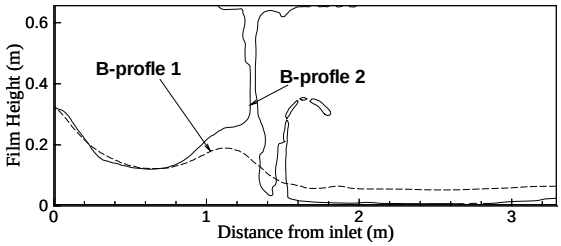

FIG. 7. The comparison of film flow shapes when B_a is in B-profile 1 and B-profile 2. AT t=0.33 sec, $\beta = 0.2$, nonconducting wall, no applied current.

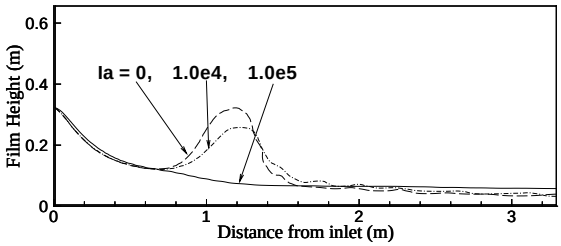

FIG. 8. The propulsion effect of the applied current. At t=0.66 sec, $\beta = 0.2$, non-conducting wall.

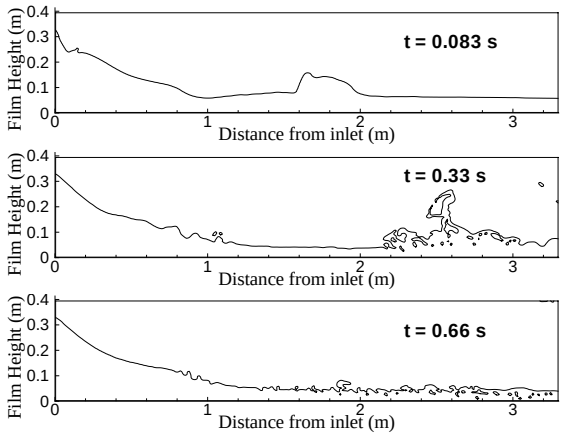

FIG. 9. The development of the film flow under propulsion effect of the applied current at large field gradient $\beta = 0.5$, $I_a = 2.5e5$A, nonconducting wall.